# 1606. Analysis on aerodynamic characteristics and noise of the high-speed train under high-speed operation

**Meng-tian Yue[1], Hong Li[2], Xin Zhou[3]**
[1]Department of Mathematics, Langfang Teachers University, Langfang, 065000, China
[2]School of Science, Hebei United University, Tangshan, 063009, China
[3]Architecture and Civil Engineering School, Inner Mongolia University of Science and Technology, Baotou, 014010, China
[1]Corresponding author
**E-mail:** [1]*lfsyky@163.com*, [2]*motain@sina.com*, [3]*zhouxin_imus@126.com*

**Abstract.** With increasingly higher operation speed of high-speed trains, air resistance will increase dramatically. Aerodynamic noise will exceed noise of the wheel-rail and become the main noise source. Numerical calculations of aerodynamic characteristics for the high-speed train under steady-state operation and tunnel-train coupling conditions were conducted in this paper. Based on the aerodynamic characteristics, distribution of aerodynamic noise on train body surface under two conditions was obtained in this paper. Furthermore, aerodynamic noise of simulated model window was extracted and compared with the experimental results. Due to good consistency, the simulated model was verified to be reliable. It is shown in both experimental and simulated results that aerodynamic noise on train body surface under tunnel-train coupling condition obviously exceeded that under steady-state operation condition. Moreover, distribution of aerodynamic noise in simulated model showed that strength of noise source on train body surface will be effectively reduced by optimizing train head. This research plays an important role in improving aerodynamic resistance and aerodynamic noise of high-speed train.

**Keywords:** high-speed trains, steady-state operation, tunnel-train coupling, aerodynamic characteristics, aerodynamic noise.

## 1. Introduction

With increasingly higher speed of high-speed train, air resistance will increase dramatically. The aerodynamic noise will be made very prominent by fluctuation of the air pressure on train body surface. For high-speed trains, Shen pointed out that noise was greatly influenced by the changes of dynamic environments [1]. Current research methods for aerodynamic characteristics and noise of high-speed trains mainly include theory research, numerical calculation and experimental research. In terms of theory research, wide influences are brought by $k$-$\varepsilon$ turbulence model and Lighthill acoustic analogy theory. They have been applied in aerodynamic characteristic analysis and noise prediction of high-speed trains. In terms of numerical calculation, George published a paper which name is Automobile Aerodynamic Noise. In the paper, he carried out comprehensive research on the aerodynamic noise source as well as generation and diffusion [2]. T. Sassa researched and analyzed the radiated noise of two-dimensional door for the high-speed train by combining large eddy simulation and boundary element [3]. Currently, there are still few researches on the aerodynamic characteristics and noise of high-speed trains. Zhang carried out experimental research on noise of a high-speed train by a multi-channel array acquisition and analysis system. He acquired the external noise level and main noise source as well as the distribution characteristics of source strength for a high-speed train under 350 km/h. His research has a very important guidance significance for the aerodynamic characteristics and noise control of high-speed trains [4]. Xiao carried out numerical calculation for the aerodynamic noises of high-speed trains under the operation speed of 200 km/h and 300 km/h respectively. The maximum frequency of the mentioned researchers was 1000 Hz, however, the aerodynamic noise of the high-speed train was a broadband noise. Hence, the frequency which was larger than 3000 Hz could not be ignored [5]. Experimental research generally consists of road test and wind

tunnel test. Experimental researches showed that the fluctuation pressure generated by the train was source of the aerodynamic noise and measures of reducing aerodynamic noise were then proposed [6-8]. However, the experimental conditions in particularly for wind tunnel test are harsh and expensive. So there are few experimental results for comprehensive and precise reference.

In the paper, aerodynamic characteristics and noise of high-speed trains under 3000 Hz were researched by combining a real road experiment with simulation. Defects of traditionally numerical calculation and wind tunnel test were overcome. Firstly, numerical calculations of aerodynamic characteristics for the high-speed train under steady-state operation and tunnel-train coupling conditions were conducted in this paper. Then, based on the aerodynamic characteristics, distribution of aerodynamic noise on train body surface under two conditions was obtained in this paper. Furthermore, aerodynamic noise of simulated model window was extracted and compared with the experimental results. Due to good consistency, the simulated model was verified to be reliable. Finally, it is shown in both experimental and simulated results that aerodynamic noise on train body surface under tunnel-train coupling condition obviously exceeded that under steady-state operation condition. Moreover, distribution of aerodynamic noise in simulated model showed that strength of noise source on train body surface will be effectively reduced by optimizing train head. This research plays an important role in improving aerodynamic resistance and aerodynamic noise of high-speed train.

## 2. Theory background

Calculation of aerodynamic characteristics and noise for high-speed trains was divided in two stages. The first stage was calculation of flow field. Firstly, the steady-state flow field was calculated by Realizable $k$-$\varepsilon$ turbulence model to acquire the basic flow field characteristics. The calculation of acoustic field was conducted at the second stage. On the basis of the calculation of the steady-state flow field, source of the aerodynamic noise for the high-speed train was calculated by a broadband noise source model.

### 2.1. Mathematical model for calculating the flow field of the high-speed train

For an operation train, its external flow field can be approximated as an incompressible viscous flow field, and the basic control equation is shown as follows:

$$\partial u_i / \partial x_i = 0, \tag{1}$$

$$\frac{\partial u_i}{\partial t} + u_j \frac{\partial u_i}{\partial x_j} = -\frac{1}{\rho}\frac{\partial p}{\partial x_i} + \frac{\mu}{\rho}\frac{\partial^2 u_i}{\partial x_j\,\partial x_j}, \tag{2}$$

where $u_i$, $u_j$ are the air velocity components in the flow field around the train. $x_i$, $x_j$ are the rectangular coordinate components. $\rho$ is the air density of the flow field around the train. $p$ is the air pressure of the flow field around the train. $\mu$ indicates the aerodynamic viscosity. $t$ is time.

A Realizable $k$-$\varepsilon$ turbulence model was used to calculate the steady-state flow field. The model was proposed by Shih [9], and it is widely used to calculate flow field such as homogeneous shear flow field, boundary layer flow field and cavity flow field.

Transport equations of the Realizable $k$-$\varepsilon$ turbulence model about $k$ and $\varepsilon$ are as follows:

$$\frac{\partial}{\partial t}(\rho k) + \frac{\partial}{\partial x_i}(\rho k u_i) = \frac{\partial}{\partial x_j}\left[\left(\mu + \frac{\mu_t}{\sigma_k}\right)\frac{\partial k}{\partial x_j}\right] + G_k + G_b - \rho\varepsilon - Y_M + S_k, \tag{3}$$

$$\frac{\partial}{\partial t}(\rho\varepsilon) + \frac{\partial}{\partial x_j}(\rho\varepsilon u_j) = \frac{\partial}{\partial x_j}\left[\left(\mu + \frac{\mu_i}{\sigma_\varepsilon}\right)\frac{\partial\varepsilon}{\partial x_j}\right] + \rho C_1 S\varepsilon - \rho C_2 \frac{\varepsilon^2}{k + \sqrt{v\varepsilon}} + C_{i\varepsilon}\frac{\varepsilon}{k}C_{3\varepsilon}G_b + S_\varepsilon, \tag{4}$$

where, $G_k$ and $G_b$ are respectively generation items of turbulence energy $k$ caused by average

velocity gradient and buoyancy. $Y_M$ refers to contribution made by pulsation expansion. $C_{i\varepsilon}$ ($i = 1, 2, 3$) is an empirical constant. $\sigma_k$ and $\sigma_\varepsilon$ are respectively Prandtl values corresponding to turbulence energy and dissipation rate. $S_k$ and $S_\varepsilon$ are source items defined by the user. $C_1$ and $A_0$ are empirical constants, wherein $C_1 = \max(0.43, \eta/\eta + 5)$, $A_0 = 4.0$. $\mu_t$ is viscosity coefficient of the turbulence flow, wherein $\mu_t = C_\mu (\rho k^2/\varepsilon)$. $C_\mu$ is a variable, $C_\mu = 1/(A_0 + A_s U^* k/\varepsilon)$, wherein the detailed expressions and derivation processes of $A_s$ and $U^*$ are shown in reference [9]. Approximate solution of $A_s$ is $A_s = \sqrt{6}\cos[1/3 \cos^{-1}(\sqrt{6}W)]$, $W = E_{ij}E_{jk}E_{ki}/(S_{ij}S_{ij})^{1/2}$, $W$ is the average rotation strain rate, and $S$ is the average strain. $U^* = \sqrt{S_{ij}S_{ij} + \widetilde{\Omega}_{ij}\widetilde{\Omega}_{ij}}$, $\widetilde{\Omega}_{ij} = \Omega_{ij} - 2\varepsilon_{ijk}\omega_k$ and $\Omega_{ij} = \overline{\Omega}_{ij} - \varepsilon_{ijk}\omega_k$.

Compared with the standard $k$-$\varepsilon$ model, two differences are mainly shown in the Realizable $k$-$\varepsilon$ turbulence model. Firstly, a formula is added in terms of turbulence viscosity. Secondly, a new equation of dissipation rate is added. This equation is derived on the basis of the fluctuation equation of laminar flow velocity. In the formula, $c_\mu$ is no longer a constant, and the contents about curvature and rotation are introduced, so as to make it meet the constraint conditions for Reynolds stress. Due to these characteristics, results of Realizable $k$-$\varepsilon$ turbulence model are made more consistent with the actual conditions in calculating pressure gradient boundary layer, rotational flow and flow separation. Currently, in numerical calculation for the external flow field of train, the calculation accuracy of Realizable $k$-$\varepsilon$ turbulence model were applied and verified [10, 11].

For selecting wall function, the Reynolds number of the near wall area on the rigid train body surface is low when the train is operating. As a result, the development of turbulence is insufficient. Its fluctuation influence is not as large as molecular viscosity $k$-$\varepsilon$ turbulence model is built for flows which turbulence develops sufficiently, and it is applicable to high Reynolds number. Therefore, wall function of semi-empirical formula should be adopted at near wall area. In other words, variables to be solved at the core area of the turbulence are associated to the physical quantities on the wall:

$$u^+ = e^\Gamma u^+_{lam} + e^{\frac{1}{\Gamma}} u^+_{turb}. \tag{5}$$

In the equation, $u^+$ is a non-dimensional velocity, $u^+ = u/v^*$. $v^*$ is shear stress velocity. $\Gamma$ is blending function, $\Gamma = -a(y^+)^4/(1 + by^+)$. $y^+$ is non-dimensional distance, $a = 0.01$ and $b = 5$.

## 2.2. Algorithm for calculating source of aerodynamic noise for the high-speed train

In many actual applications considering turbulence, continuous distribution in a broadband range is presented for the noise energy, which involves in broadband noise. Few calculation resource is consumed by the broadband acoustic source model. The strength of the noise source on the solid surface wall of the flow field can be quickly analyzed and preliminarily predicted by it. Under broadband noise source model, the noise energy generated in the entire flow field can be defined by quantizing the local contribution, and the noise source can be analyzed and extracted. In this way, the main factors for noise generation can be known. The currently common Proudman model was selected.

The generated acoustic energy by the isotropic turbulence is as follows:

$$P_A = \alpha\rho_0 \left(\frac{u^3}{l}\right)\frac{u^5}{a_0{}^5}. \tag{6}$$

For $k$ and $\varepsilon$, the mentioned formula can be written as:

$$P_A = \alpha_\varepsilon \rho_0 \varepsilon M_t{}^5. \tag{7}$$

The sound power level is as Eq. (8):

$$L_p = 10\log\left(\frac{P_A}{P_{ref}}\right), \tag{8}$$

where, $u$ is turbulence velocity. $l$ is characteristic length. $a_0$ is sound velocity. $\alpha$ is model constant. $M_t = \sqrt{2k}/a_0$.

According to the mentioned theory analysis, problem of the flow field noise can be predicted by the Proudman noise energy approximation formula based on the premise of high Reynolds number and low Mach number. The flow of the train during steady operation basically meets the requirement.

## 3. Preparations for physical model

### 3.1. Model simplification

Limited by computer hardware, the real movement condition of the train cannot be completely simulated by the calculation model. Therefore, the calculation model needs to be simplified. The model is subject to the followed simplifications during building.

1) Three trains were simulated in this paper. In other words, the entire model consisted of a head train, a middle train and a tail train. The head train and the tail train had identical appearance.

2) Pantograph, bogie, wheels and the small devices under the train were removed. Meanwhile, according to the symmetry, half of the model was cut along the longitudinal symmetrical plane of the train body to save computer resource.

3) Operation condition was uniform linear motion without considering wind. Operation velocity was approximate 250 km/h.

4) Compressibility of air was ignored. The air could be considered as incompressible viscous fluid when the Mach number was less than 0.3, and such condition had a little error.

5) A cross-section of common single track railway was used as the tunnel, as shown in Fig. 1. The simplification result of its profile was as shown in Fig. 2.
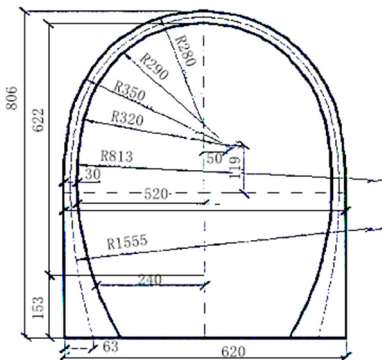


**Fig. 1.** Cross-section of the tunnel for common single track railway
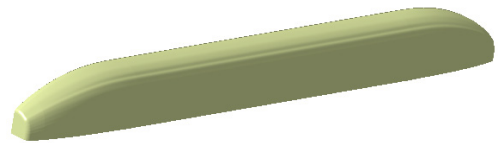
**Fig. 2.** The geometrical model of a train

### 3.2. Boundary conditions, mesh generation and calculation

#### 3.2.1. High-speed steady-state condition

The simplified three-dimensional model was imported into Gambit and T-Grid to generate

mesh. A calculation domain with the length of 300 m, width of 11.5 m and height of 18 m was built. The entire calculation domain was divided into four parts by structured mesh. Such method was conducive to improving the calculation accuracy. Number of the mesh was 300,000. Then, boundary definition was carried out, and the front and back boundary was pressure-far-field. The bottom boundary was move-wall, and the upper and bottom surfaces of the train body model were walls. They were used for subsequent calculation and description of air flow field characteristics. The calculation mesh is as shown in Fig. 3 and Fig. 4.
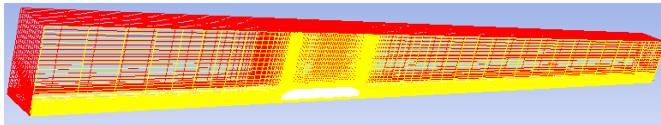


**Fig. 3.** Planning of the flow field calculation domain outside the train
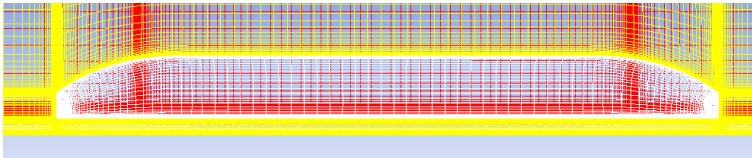


**Fig. 4.** Mesh of the flow field near the train body

During calculation of the steady-state flow, the turbulence model used Realizable $k$-$\varepsilon$ model. Some history effect was included in the turbulence viscosity coefficient of this model [12]. Turbulence viscosity coefficient as well as turbulent kinetic energy and its dissipation rate could be associated by it. Hence, the calculation accuracy of numerical simulation could be improved significantly. The enhanced wall function was taken as near wall function, and separation solver was taken as the solver. Compressible flow analysis was built by double precision solving, second order upwind scheme. SIMPLEC algorithm was adopted in the coupling calculation of pressure and velocity. In this way, the convergence solutions such as $p$, $u$, $v$ etc. of the flow field parameters could be acquired through iteration. Hence, a high calculation accuracy and stability could be obtained.

### 3.2.2. Train-tunnel coupling condition

The domain of tunnel-train flow field was 100 m long. The entrance of flow field was 26 m away from the head of the train. The train body surface and the tunnel surface were triangle mesh. The calculation domain was tetrahedral mesh. The number of space volume mesh elements was 1.2 million as shown in Fig. 5. The front and back boundary was pressure-far-field, and the tunnel boundary was move-wall. The upper and bottom surfaces of the train body model were walls. They were used for subsequent calculation and description for air flow field characteristics.
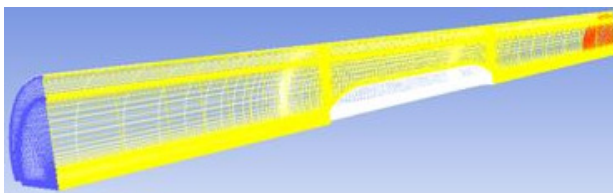


**Fig. 5.** Flow field mesh of tunnel-train

### 4. Numerical calculation of aerodynamic characteristics

Aerodynamic characteristics under high-speed steady-state condition and train-tunnel coupling condition were simulated, respectively.

## 4.1. Analysis on the results of the external flow field for the train under steady-state

Air resistance of the train was 0.131, and aerodynamic lift was 0.98. The air moment against the head was –0.466. Meanwhile, according to Fig. 6-Fig. 9, when the train was under high-speed steady-state operation, the head was facing the stream. The air flow was prevented at the arc top. Hence, the velocity decreased significantly, almost reaching 0, as shown in Fig. 8.
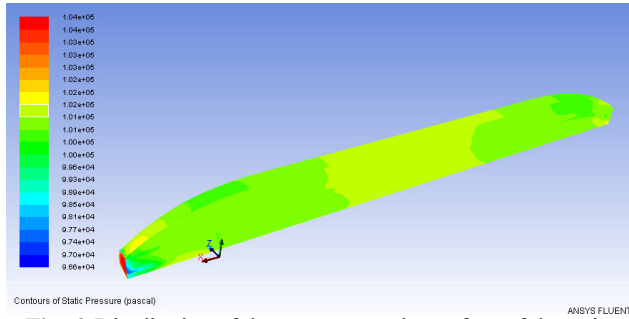


**Fig. 6.** Distribution of the pressure on the surface of the train
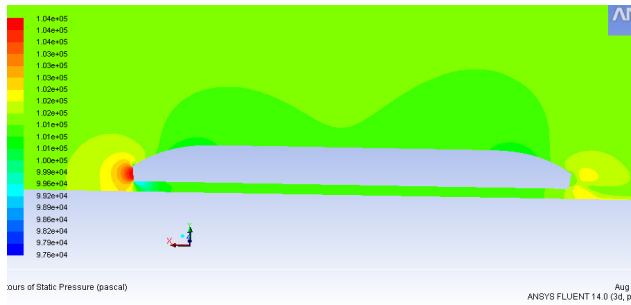


**Fig. 7.** Distribution of the pressure in the external flow field of the train
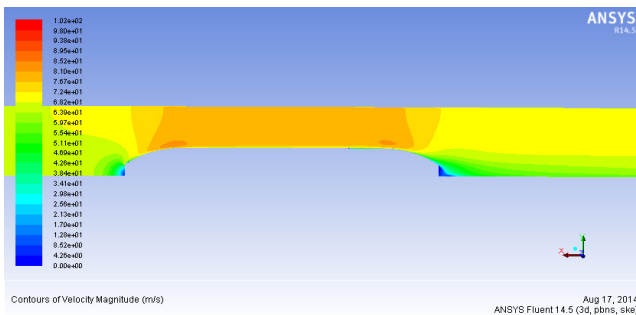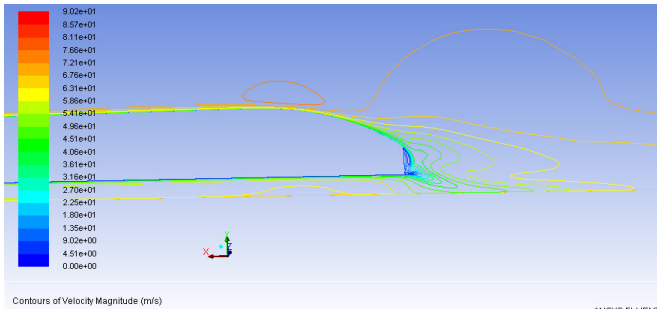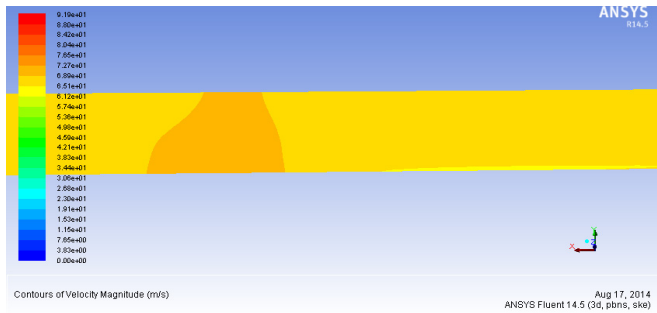


**Fig. 8.** Velocity vector of the external flow field for the train

The flow field at the head was in positive pressure status. Meanwhile, the velocity of the external flow field reached the first negative pressure peak at the maximum cross-section of the train. Some air flow moved backward along both sides of the train and the upper curved surface. The flow velocity was accelerated by the change of curvature from the head to the train body. The positive pressure gradually decreased until it became negative pressure. The negative pressure reached maximum value at the head and the side surface. The second velocity peak occurred at the tail of the train, which was generated due to the acceleration of air flow velocity and the influence of the flow. The maximum velocity of flow field outside the train body reached 72.7 m/s. According to Fig. 10, when the maximum velocity was 4.7 m/s < 14 m/s, passengers could bear

at the position which was 2 m away from the train body. Such condition met the requirements of safe for human body.



**Fig. 9.** Velocity curve of the flow field at the tail of the train



**Fig. 10.** Velocity characteristics of the side for the train body

## 4.2. Analysis on the external flow field of the train under train-tunnel coupling

Air resistance of the train was 0.165, which was larger than the air resistance of steady-state condition, and aerodynamic lift was 3.75. Air moment against the head was –1.87. According to Fig. 11-Fig. 13, the tunnel wall near the head was positive pressure area. At this position, the value reached maximum peak. The pressure on the tunnel wall opposite to the train body distributed uniformly, and it was negative pressure area. Due to the prevention of the head, the air flow velocity decreased significantly, almost reaching 0 when the air flow passed the surface of the train.
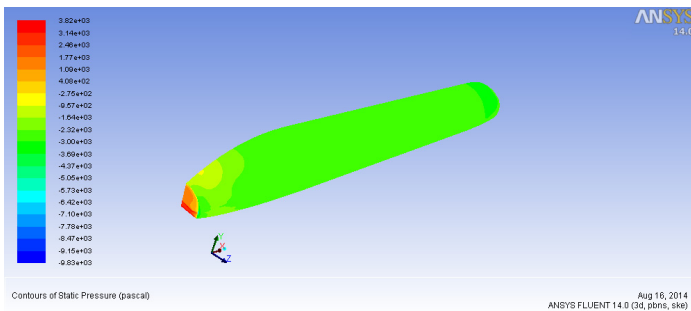


**Fig. 11.** Distribution of the pressure on the train surface in tunnel environment

Comparison with the aerodynamic characteristics in steady-state condition in Section 4.1.1 showed that the train suffered from larger resistance in tunnel environment than steady-state condition. The exceeded resistance was the additional air resistance in the tunnel. The resistance was caused by the pressure difference between the positive pressure at the head and the negative

pressure at the tail. It was because the air was driven by the train when it entered into the tunnel. Hence, resistance was generated. Meanwhile, because of the train structure, turbulence flow will be caused by the air in the tunnel. Friction between the air and the train surface as well as the tunnel surface will be caused by the flow. Therefore, resistance resisting the train's motion will be generated. The longer the tunnel is, the larger the resistance will be. The longer the train is, the larger the velocity will be, and the resistance will increase accordingly. In addition, this resistance is also related to the sectional area of the tunnel, train appearance etc.
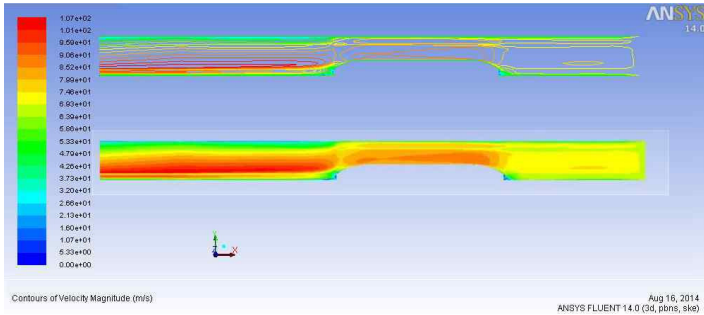


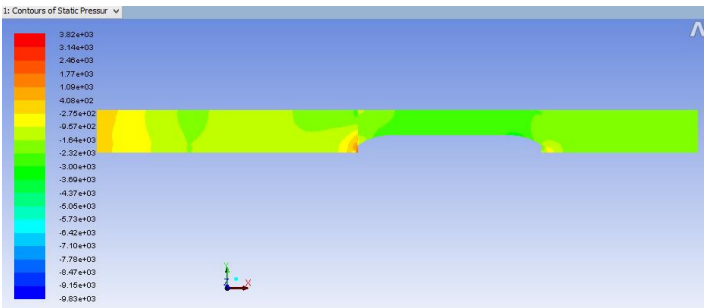**Fig. 12.** Distribution and curve of the flow field velocity in the tunnel



**Fig. 13.** Distribution of the pressure of the external flow field for the train in the tunnel

## 5. Numerical calculation and experimental research of aerodynamic noise

High-speed train is a complicated model. Results of its aerodynamic noise may not be accurate if the research is conducted directly by a numerical method. Hence, accuracy of the numerical calculation model shall be verified by experiment.

### 5.1. Experimental research of aerodynamic noise

PULSE analyzer of B&K Company was used as test equipment in aerodynamic noise experiment of the high-speed train. During the test of the external sound pressure for a high-speed train under high-speed operation condition, a traditional microphone could not be used to obtain the accurate experimental results. Hence, an aviation microphone was installed on the outer surface of the train window to test the external sound pressure, as shown in Fig. 14. In this way, the accurate experimental results could be obtained under high-speed operation. Test process of the external sound pressure was shown in Fig. 15. A multi-channel signal collection equipment was used to obtain signals of microphone. Then, the obtained data signals were imported into a PULSE analyzer for processing. Sound pressure levels of train body surface under steady-state operation and tunnel-train coupling conditions were tested, respectively, as shown in Fig. 16 and Fig. 17.

It is shown in Fig. 16 and Fig. 17 that sound pressure of train body surface under the tunnel-train coupling condition exceeded that under the steady-state operation condition within the whole frequency range. It was mainly because that strong coupling was generated between train and tunnel
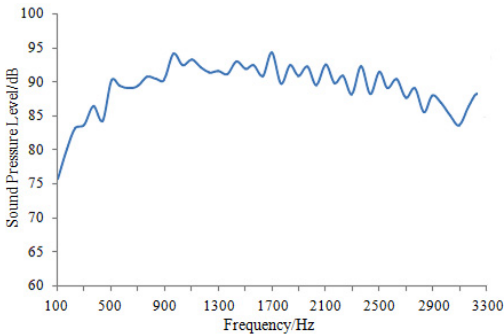
during train operation. As a result, sound pressure of train body surface was strengthened.
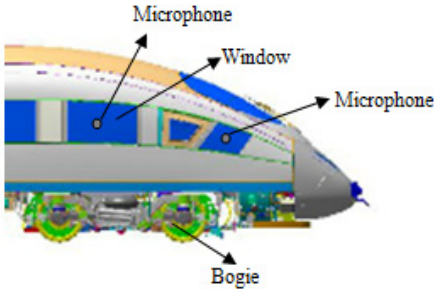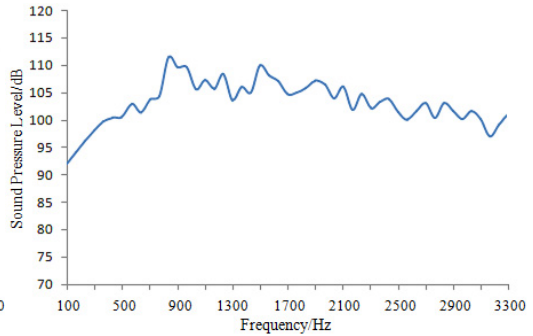


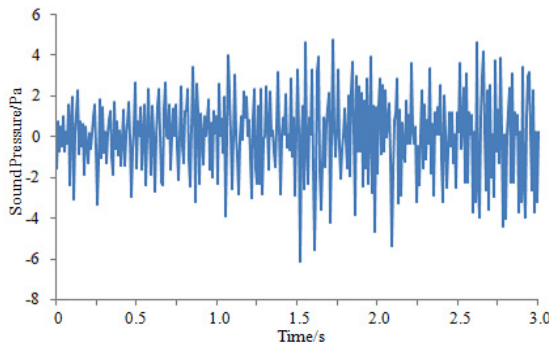**Fig. 14.** Installation diagram of the high-speed train microphone
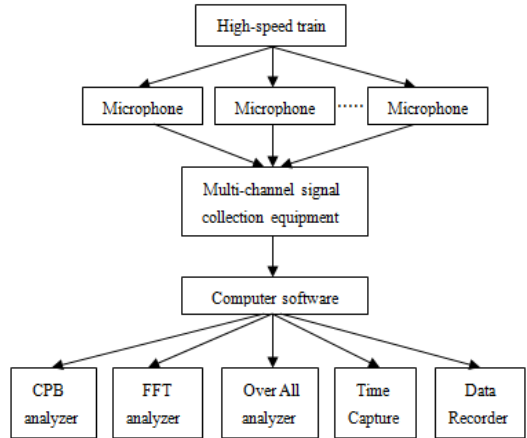


**Fig. 15.** Test process of the external sound pressure for the high-speed train



**Fig. 16.** Sound pressure level of train body surface under steady-state operation condition



**Fig. 17.** Sound pressure level of train body surface under tunnel-train coupling condition



**Fig. 18.** Relationship between sound pressure of train body surface and time when it went through a tunnel

Signals which were obtained by the multi-channel data collection equipment were imported into Sound Quality software. And then, a curve for sound pressure of train body surface with time when a high-speed train entered into a tunnel under the operation speed of 250 km/h, as shown in Fig. 18. It is shown in the figure that fluctuation amplitude of the sound pressure curve suddenly increased at the time point of 1.5 s. On the one hand, air flow sound sharply increased at the instant when the train entered into the tunnel. On the other hand, the tunnel is equivalent to space with

two opened ends while its inner wall surfaces are made of hard materials with very high reflection coefficients. As a result, the noise was much higher than that outside the tunnel. Such conclusion is consistent with the mentioned analysis results.

## 5.2. Numerical calculation of aerodynamic noise

Based on flow field of train body surface under steady-state operation condition, all parameters were consistent with experimental results, and then, numerical calculation was conducted to obtain sound power level of train body surface under the condition, as shown in Fig. 19.
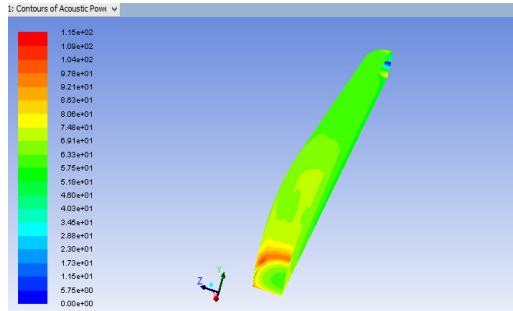


**Fig. 19.** Distribution of sound power level of the train body under steady-state operation condition
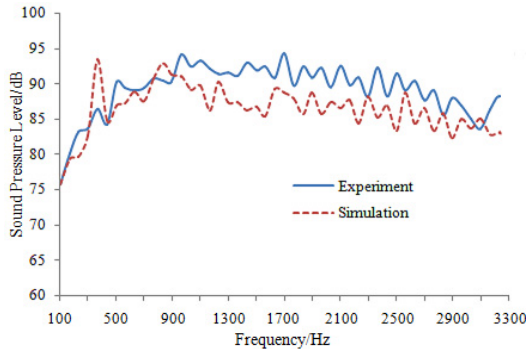


**Fig. 20.** Experimental and simulated comparison of sound pressure level of train body surface under steady-state operation condition

Sound power of train window in Fig. 19 was extracted, and it was transformed into sound pressure level and compared with experimental results in Fig. 16, as shown in Fig. 20.

It is shown in Fig. 20 that great differences were not shown by experimental results and simulated results in the whole analysis frequency range. In addition, the variation trends of experimental and simulated curves were consistent. Hence, the simulation model was deemed to be reliable, and it can be used to effectively predict aerodynamic noise of the high-speed train under steady-state operation.

According to Fig. 19, air flow speed increased due to the change of curved surface at the head. Because of the interaction between the boundary layer of the train body surface and the external flow field, the noise was high. Therefore, optimizing the shape of the head part for the train is an effective method to reduce the aerodynamic noise.

Sound power distribution of train body surface under the tunnel-train coupling state was obtained as shown in Fig. 21.

According to the method for obtaining sound power levels of train body surface under the steady-state operation condition. Sound powers at train window in Fig. 21 were extracted, and it was transformed into sound pressure levels and compared with experimental results in Fig. 17, as

shown in Fig. 22.

It is shown in Fig. 22 that experimental results were relatively bigger than simulated results at frequencies of 900 Hz and 1500 Hz. It was because that certain error might be included in experimental results during test under so complicated environment. However, great differences were not shown in experimental and simulated results for the most frequencies within the whole frequency range. Moreover, the variation trends of both of them were basically consistent. Hence, the simulation model was deemed to be reliable, and it can be used to predict aerodynamic noise under tunnel-train coupling condition.
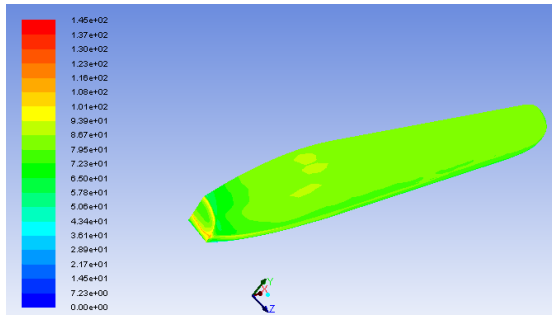


**Fig. 21.** Distribution of sound power level of the train body under tunnel-train coupling condition
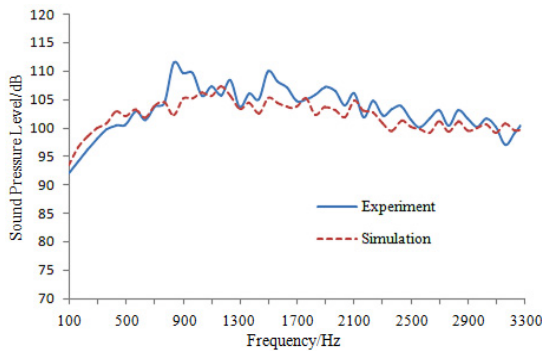


**Fig. 22.** Experimental and simulated comparison of sound pressure level of train body surface under tunnel-train coupling condition

It is shown in Fig. 21 that sound power distribution of train body surface under this condition was basically consistent with that under steady-state condition. Hence, aerodynamic noise can be reduced by optimizing the train head.

## 6. Conclusions

1) The aerodynamic positive pressure area on the train body surface is mainly distributed on the head which firstly gets contact with the front steady air flow. While, the negative pressure area is the middle part of the train body, while the air flow is smooth there. Under the function of air viscosity, mutual interactions are brought by the ground effect and the boundary layer on the surface. Therefore, tail swirling vortex field at the train tail is formed.

2) In tunnel environment, the aerodynamic characteristics and features of the air flow field around the train body are significantly different from that under steady-state condition. Tunnel effect is significant. The compressible flow status of the air is strengthened by the tunnel wall, and the flow field velocity and turbulence extent are also accelerated by it.

3) It is shown in experimental results that the train surface sound source is stronger under tunnel-train coupling condition than that under steady-state operation condition due to coupling.

Moreover, experimental and simulated results were relatively consistent under two operation conditions, and the simulation model can be used to predict the actual aerodynamic noise of the train.

4) It is shown in simulated results that distribution of the train noise source was approximately same under two operation conditions and aerodynamic noise can be effectively reduced by optimizing the train head.

## References

**[1]** **Shen Z. Y.** Dynamic environment of high-speed train and its distinguished technology. Journal of the China Railway Society, Vol. 28, Issue 4, 2006, p. 1-5.

**[2]** **Sassa T., Sato T., Yatsui S.** Numerical analysis of aerodynamic noise radiation from a high-speed train surface. Journal of Sound and Vibration, Vol. 247, Issue 3, 2001, p. 407-416.

**[3]** **George A.** Automobile aerodynamic noise. SAE Technical Paper 900315, 1990.

**[4]** **Zhang S. G.** Noise mechanism, sound source localization and noise control of 350 km/h high-speed train. China Railway Science, Vol. 30, Issue 1, 2009, p. 86-90.

**[5]** **Xiao Y. G., Kang Z. C.** Numerical prediction of aerodynamic noise radiated from high speed train head surface. Journal of Central South University (Science and Technology), Vol. 39, Issue 6, 2008, p. 1267-1272.

**[6]** **Fedmion N., Vincent N.** Aerodynamic noise radiated by the intercoach spacing and the bogie of a highspeed train. Journal of Sound and Vibration, Vol. 231, Issue 3, 2000, p. 577-593.

**[7]** **Kitagawa T., Nagakurak K.** Aerodynamic noise generated by shinknsen cars. Journal of Sound and Vibration, Vol. 231, Issue 3, 2000, p. 913-924.

**[8]** **Noger C., Patrat J. C., Peube J., et al.** Aeroacoustical study of the TGV pantograph reccess. Journal of Sound and Vibration, Vol. 231, Issue 3, 2000, p. 563-575.

**[9]** **Shih T.-H., Zhu J., Lumley J. L.** A New Reynolds Stress Algebraic Equation Model. NASA TM, 106644, 1994.

**[10]** **Pan X. W., Gu Z. Q., He Y. B., Wang Y. P.** CFD Simulation and experimental study on the aerodynamic characteristics of a F1 racing Car. Automotive Engineering, Vol. 31, Issue 3, 2009, p. 274-277.

**[11]** **Liang J. Y., Liang J.** Comparison among turbulence models in CFD analysis on flow field around a car. Automotive Engineering, Vol. 30, Issue l, 2008, p. 846-852.

**[12]** Fluent Inc. Fluent User's Guide, 2005.

**Mengtian Yue** received M.S. degree in Management from Hebei University of Technology, Tianjin, China, in 2010. Now he works in Department of Mathematics and Information Science, Langfang Teachers University. His current research interests include computational mechanics and dynamics.



**Hong Li** received her Master degree in Tianjin University, she is an Associated Professor in Heibei University, Tangshan, China. Now her current research interests include detecting mechanical properties and electrical performance with experimental device, photometry and colormetry on improving lighting quality.



**Xin Zhou** is studying for a Master degree in Architecture and Civil Engineering Institute from Inner Mongolia University of Science and Technology, Baotou, China. His current research interests include improvement of furnace slag, particle flow code and building material for foundations.